Smart Structures and Systems, *Vol. 27, No. 3 (2021) 547-557*
DOI: https://doi.org/10.12989/sss.2021.27.3.547

An efficient approach for optimum shape design of steel shear panel dampers under cyclic loading

Mohsen Khatibinia*[1], Aghdas Ahrari [1b], Sadjad Gharehbaghi [2c] and Seyyed Reza Sarafrazi [1d]

[1] *Department of Civil Engineering, University of Birjand, Birjand, Iran*
[2] *Department of Civil Engineering, Sharif University of Technology, Tehran, Iran*

(*Received February 18, 2020, Revised September 15, 2020, Accepted December 21, 2020*)

Abstract. The low-cycle fatigue performance of shear panel damper (SPD) highly depends on the geometry of its shape and the criterion considered for its design. The main contribution of the current study is to find the optimum shape of the SPD subjected to cyclic loading by considering two different objective functions. The maximum equivalent plastic strain and the ratio of energy dissipation through plastic deformation to the maximum equivalent plastic strain are selected as the first and second objective functions, respectively. Since the optimization procedure requires high computational efforts, a hybrid computational approach is used to perform two paramount phases of estimating the inelastic responses of the SPD and solving the optimization problem. In the first phase, as an alternative for the time-consuming finite element analysis of the SPD, a weighted-support vector machine model is developed to predict the inelastic responses of the SPDs during the optimization process. In the second phase, the optimum shape of the SPD is found by using the whale optimization algorithm (WOA). The results indicate that both design criteria lead to the optimum-shaped SPDs with a significant improvement in their low cycle fatigue performance in comparing with the initial rectangular shape while a slight reduction in their energy dissipation capacity. Moreover, the second design criterion is slightly better in the performance improvement of the optimum-shaped SPDs compared with the first one. In addition, the weighted-based SVM approach can accurately predict the inelastic responses of the SPDs under cyclic loading, and its combination with WOA results in finding the optimum solutions quickly.

Keywords: shear panel damper; energy dissipation; shape optimization; support vector machine; whale optimization algorithm

1. Introduction

In general, the structural design is a trade-off between minimizing the construction cost and maximizing the structural safety (Gharehbaghi 2018). In recent years, civil engineers have conducted many efforts for the design of resilient structures. To this end, one way is to increase the robustness and the recovery time of a structure after occurring a natural hazard such as earthquake. To achieve this goal, the dissipative devices, the capable of dissipating seismic energy and avoiding damage to main structural elements, can be used to improve the seismic performance of the structural systems (Wong 2008, Xu *et al*. 2017, Bilondi *et al*. 2018, Khatibinia *et al*. 2019). This idea results in increasing the structural robustness and, indeed, mitigating or even removing the damage of main structural elements. In addition, the dissipative devices can be replaced quickly for early recovering of the structural functionality. One type of the devices is metallic dampers such as added damping and stiffness (ADAS) and triangular added damping and stiffness (TADAS) elements (Mahmoudi and Abdi 2012, Saeedi *et al*. 2016, Sorace *et al*. 2016), U-shaped steel dampers (USSDs) (Kishiki *et al*. 2008, Jiao *et al*. 2015, Ene *et al*. 2016), shear panel dampers (SPDs) (De Matteis *et al*. 2009, Kang *et al*. 2013, Jain *et al*. 2008, Hamed and Mofid 2015, Akbari and Mofid 2015, Zhang *et al*. 2016) and SPDs with openings (Vian *et al*. 2009, Valizadeh *et al*. 2012, Chan *et al*. 2013, Egorova *et al*. 2014, De Matteis *et al*. 2016). In recent decades, the effectiveness of the devices has been proved in enhancing the structural safety of buildings and bridges subjected to large earthquakes. It is worth mentioning that they are required to be optimally designed and located at a zone to dissipate the seismic input energy, as well as they should be replaceable.

The SPDs as the passive damping devices are typically made of low yield steel material. The advantages of the SPDs include their suitable cost and energy dissipation capacity. Hence, the devices have been extensively utilized for the seismic performance improvement of structures (Hossain *et al*. 2011, Choi and Park 2010). The typical application of the SPDs in a bridge and a framed building is shown in Fig. 1.

In addition, the SPDs should show excellent plastic deformations due to the possible shear deformations during a strong earthquake. To enhance the large demand of shear

*Corresponding author, Associate Professor,
E-mail: m.khatibinia@birjand.ac.ir
[a] Ph.D.
[b] M.Sc. Student
[c] Ph.D. Student
[d] Ph.D.

ISSN: 1738-1584 (Print), 1738-1991 (Online)

deformation in the design of bridge and building structures under severe earthquakes, the proper design of the SPDs is necessary to guarantee its deformation and energy dissipation capability (Liu *et al*. 2007). The plastic strain concentration can be observed because of an inappropriate design which results in initiating cracks on edges or corners of the SPDs during a severe earthquake (Liu *et al*. 2007).

Several studies have been conducted for the performance improvement of the low cycle fatigue in the SPDs. The effects of material type, the arrangement of stiffeners and the shape of the SPDs are the main topics of the conducted studies. Nakashima *et al*. (1994) investigated the cyclic behavior of the SPDs made of the low-yield steel material. The results of their study proved that the low cycle fatigue performance of the SPDs is significantly enhanced by using the low yield steel in comparison with the ordinary steel material. Other studies (Rai *et al*. 2013, De Matteis *et al*. 2008, 2011, Sahoo and Rai 2013, Brando and De Matteis 2014) demonstrated the effectiveness of low yield steel or aluminum alloy in the construction of the SPDs. Ohsaki and Nakajima (2012) found an optimum arrangement for the stiffeners of a SPD to maximize its energy dissipation capacity. By this way, the maximum equivalent plastic strain was significantly reduced, and the low cycle fatigue performance was increased. The effect of the SPDs shape on their cyclic performance was investigated using a set of experimental tests (Zhang *et al*. 2012a, b). Their results showed that weakening the center of a SPD could improve its deformation capacity and low cycle fatigue performance compared with that of the conventional one. Liu and Shimoda (2013) presented the optimum shape of the SPDs using the response surface methodology. In their study, the edge of the SPD was shaped based on the cubic Bezier curve, and the maximum energy dissipation through plastic deformation was considered as the objective function to be minimized. Although their idea was resulted in the performance improvement of the SPDs, the methodology presented in this study was not necessarily reached a global optimum solution and required much computational burden as well. Deng *et al*. (2014) presented a study on the shape optimization of the SPDs using a simulated annealing algorithm. The results of this study indicated that the equivalent plastic strain of the optimum shape design for the SPD was distributed more uniformly in comparing with that of the conventional rectangular SPD. In their work, the energy dissipation capability of the SPD was not considered as a main factor of the optimization problem defined.

By taking a glance at literature, it seems that further studies are required to enhance the seismic performance of the SPDs. One solution is to reach a global optimum shape for these dampers. For this purpose, defining a performance criterion is of crucial importance. The main contributions of this study include: (1) assessing the effect of two performance criteria in finding the optimum shape of the SPDs under cyclic loading, (2) presenting an efficient hybrid approach to reduce the computational efforts required for implementing the shape optimization process. To achieve this end, two performance criteria are proposed as the objective functions of the shape optimization problem. The maximum equivalent plastic strain is selected as the first objective function to be minimized, and the ratio of energy dissipation through plastic deformation to the maximum equivalent plastic strain is considered as the second objective function to be maximized. To find the optimum solution, an efficient computational approach including a meta-heuristic optimization algorithm and a soft computing-based response predictive tool is adopted. The whale optimization algorithm (WOA) (Mirjalili and Lewis 2016) is used for finding the optimum shape of the SPD. Determining the inelastic cyclic responses of a finite element model (FEM) of the SPDs subjected to cyclic loading requires an expensive computational effort. This issue is accentuated because of using an iterative optimization process. To eliminate the problem, a weighted least squares support vector machine (WLS-SVM) (Suykens *et al*. 2002), as a robust predictive tool, is employed for the precise prediction of the inelastic responses of the SPD model under cyclic loading. The combination of WOA and WLS-SVM not only results in an optimum shape for the SPDs with the improved performance but also reduces the computational cost of the optimization procedure. The shape optimization problem, the hybrid computational approach, numerical examples and findings are described in the next sections.

2. Shape optimization of SPD

Shape optimization is one of the main steps of structural design problems which, in turn, can significantly affect the performance of the final design solution. The shape optimization design deals with the determining the exterior and interior boundaries of a structure (Olhoff 1995). In the current work, the optimum dimensions of the SPDs

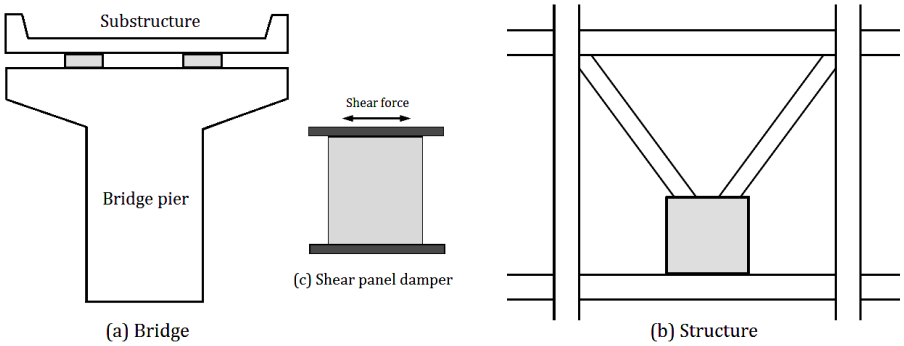

Fig. 1 Application of SPD for (a) a girder bridge as bearing; (b) the brace frame

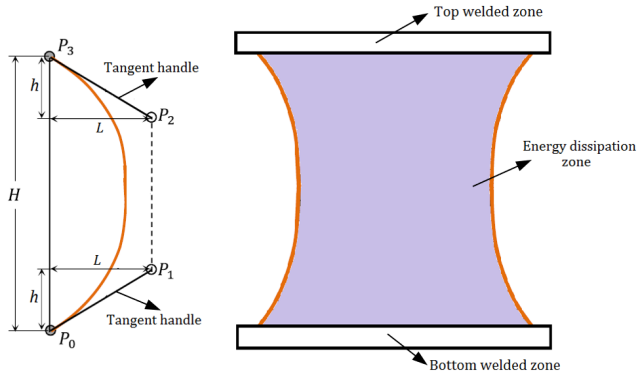

Fig. 2 Shape parameterization of the SPD using the Bezier curve

subjected to cyclic loading were determined.

2.1 Geometry of SPD shape

In the experimental studies carried out by Liu *et al.* (2007) and Aoki *et al.* (2007), it was demonstrated that the arc-shaped free edges on the left and right sides of the SPDs substantially affect their deformation capacity (i.e., the low cycle fatigue performance). Accordingly, in the current study, the geometry of these edges was considered as the variable of the shape optimization problem. A geometry conformed to a cubic Bezier curve (Faux and Pratt 2003) was considered to be found optimally. The cubic Bezier curve is consisted of a set of control points including the anchor points as P_0, P_3 and the handle points as P_1, P_2. As shown in Fig. 2, the explicit form of the cubic Bezier curve represented by $B(t)$ can be expressed by the control points as follow (Liu and Shimoda 2013)

$$B(t) = (1-t)^3 P_0 + 3(1-t)^2 t P_1 + 3(1-t)t^2 P_2 + t^3 P_3 \quad (1)$$

where t is an intermediate point ranging from 0 to 1. Since the equivalent plastic strain distribution on the upper and lower half of the SPD is symmetry, the coordinates of the control points P_0, P_1, P_2, P_3 are defined as (0,0), (L,h), (L,H-h) and (0,H), respectively (see Fig. 2).

2.2 Shape definition of optimization problem

The definition of the cubic Bezier curve depends on the parameters of L and h which are seen in Fig. 2. In this study, these parameters were selected as the design variables of the shape optimization problem. Mathematically, the shape optimization formulation of the SPD can be expressed as

$$\begin{aligned} &\text{Find: } \boldsymbol{x} = \{L, h\} \\ &\text{Minimize or Maximize: } F(\boldsymbol{x}) \\ &\text{Subjected to: } L_{min} \le L \le L_{max} \\ &\qquad\qquad\quad h_{min} \le h \le h_{max} \end{aligned} \quad (2)$$

where F is the objective function. $L_{\min}$ and $L_{\max}$ are the lower and upper bonds of L parameter; $h_{\min}$ and $h_{\max}$ are the lower and upper bonds of h parameter.

The efficiency and performance of the SPD highly depends not only on its shape (i.e., L and h), but also on the inelastic response of the SPD which is selected as the design criterion (i.e., as the objective function in this study). As such, this study assesses the suitability of two objective functions for finding the optimum shape of the SPD under cyclic loading. The objective functions include: (1) The maximum equivalent plastic strain (denoted hereinafter as $PEEQ_{\max}$) is considered as the first objective function to be minimized, and (2) the ratio of energy dissipation through plastic deformation (denoted hereinafter as *ALLPD*) to $PEEQ_{\max}$ is considered as the second objective function to be maximized. For simplicity, the first and second objective functions are abbreviated as F_1 and F_2. Finally, the objective functions can be expressed as

$$\text{Minimize: } F_1(\boldsymbol{x}) = PEEQ_{max} \quad (3)$$

$$\text{Maximize: } F_2(\boldsymbol{x}) = \frac{ALLPD}{PEEQ_{max}} \quad (4)$$

3. Whale optimization algorithm

The Whale Optimization Algorithm (WOA) as a novel meta-heuristic algorithm was proposed by Mirjalili and Lewis (2016), which was simulated based on the social behavior in humpback whales. This algorithm is implemented based on the spiral bubble-net feeding maneuver. For updating the position of the whales during the optimization procedure, the shrinking encircling mechanism and the spiral bubble-net feeding maneuver are used. In the basic WOA, it is assumed that the current best solution candidate can be considered as the optimum or near optimum. Hence, the position of other search agents is updated towards the best search agent (Mirjalili and Lewis 2016).

The WOA includes two phases of exploitation and exploration, and also transits between them smoothly. The transition is implemented by the value variation of $\boldsymbol{A}$ vector. The value of $\boldsymbol{A}$ vector is decreased in each iteration, and in half of the iterations it is assigned to exploration phase when $|\boldsymbol{A}| \ge 1$ and the rest is dedicated to exploitation when $|\boldsymbol{A}| < 1$. Herein, the sign $|\ |$ is considered as the absolute value. The vector $\boldsymbol{A}$ is computed as follow

$$\boldsymbol{A} = 2\boldsymbol{a}\boldsymbol{r} - \boldsymbol{a} \quad (5)$$

where $\boldsymbol{a}$ is linearly decreased from 2 to 0 during the optimization procedure, and $\boldsymbol{r}$ is a random vector in [0,1].

3.1 Bubble-net attacking method (exploitation phase)

For modeling the bubble-net behavior of humpback whales, two schemes including shrinking encircling mechanism and spiral updating position were proposed (Mirjalili and Lewis 2016). Since the humpback whales simultaneously can swim around the prey through a shrinking circle and along a spiral-shaped way, it is assumed in WOA that a probability of 50% is selected

between the two behaviors. The shrinking encircling mechanism is simulated as follow

$$\bar{\boldsymbol{C}} = 2\boldsymbol{r} \tag{6}$$

$$\boldsymbol{D} = |\boldsymbol{C}\,\boldsymbol{X}^*(l) - \boldsymbol{X}(l)| \tag{7}$$

$$\boldsymbol{X}(l+1) = \boldsymbol{X}^*(l) - \boldsymbol{A}\,\boldsymbol{D} \tag{8}$$

where $\boldsymbol{X}$ is the position of whales, and $\boldsymbol{X}^*$ is the position vector of the best solution obtained from the first iteration to current iteration. Moreover, the spiral-shape movement of whales is simulated as following formulas

$$\boldsymbol{D}' = |\boldsymbol{X}^* - \boldsymbol{X}(l)| \tag{9}$$

$$\boldsymbol{X}(l+1) = \boldsymbol{D}' e^{bp} \cos(2\pi p) + \boldsymbol{X}^* \tag{10}$$

where b is a constant that define the spiral shape of movement. p is a random number in [–1,1].

3.2 Search for prey (exploration phase)

In the exploration phase of WOA, the position of a whale is updated based on a randomly chosen whale instead of the best search whale. Thus, the new position of whales is obtained as

$$\boldsymbol{D} = |\boldsymbol{C}\,\boldsymbol{X}^*(l) - \boldsymbol{X}(l)| \tag{11}$$

$$\boldsymbol{X}(l+1) = \boldsymbol{X}^*(l) - \boldsymbol{A}\,\boldsymbol{D} \tag{12}$$

4. Modeling and verification of SPD

In this study, modeling and analyzing of the SPD was implemented by using the finite element (FE) method. The process and verification of modeling the SPD are briefly expressed in this section.

4.1 FE modeling procedure of SPD

In this paper, ABAQUS software package (ABAQUS 2003) was used for modeling and analyzing the FE model of the SPD. For this purpose, the 4-node shell element with reduced integration and hourglass control (so-called S4R in ABAQUS) was selected for meshing the FE model of the SPD. The cyclic behavior of the SPD material was simulated by the combination of the isotropic and kinematic hardening. In the numerical scheme of the material law, the kinematic hardening as a nonlinear component is explained by superimposing two or more nonlinear models of the kinematic hardening as (Jirasek and Bazant 2001)

$$\alpha = \sum_{k=1}^{n} \frac{C_k}{\gamma_k}\left(1 - e^{-\gamma_k \varepsilon^{pl}}\right) \tag{13}$$

which n is the number of back-stresses; C and γ are considered as the material parameters, which should be calibrated by using the data of a cyclic test. C is the initial module of the kinematic hardening. The module of the kinematic hardening with increasing plastic deformation is decreased by a rate which is determined by γ. ε^{pl} is the equivalent plastic strain (i.e., *PEEQ*).

The size of the yield surface material is assessed by the component of the isotropic hardening, which is obtained as follows (Lemaitre and Chaboche 1994)

$$\sigma^0 = \sigma_0 + Q_\infty\left(1 - e^{-b\varepsilon^{pl}}\right) \tag{14}$$

where σ_0 is the initial yield stress which is occurred at zero plastic strain; Q_∞ and b are considered as the material parameters. Q_∞ is the maximum change in the yield surface size.

In order to obtain *ALLPD*, a post-processing is implemented on the ABAQUS outputs. Thus, *ALLPD* is calculated as follows (ABAQUS 2003)

$$ALLPD = \int_V \int_0^{\bar{t}} \boldsymbol{\sigma} : \dot{\boldsymbol{\varepsilon}}^{pl} d\bar{t} dV \tag{15}$$

where $\boldsymbol{\sigma}$ and $\dot{\boldsymbol{\varepsilon}}^{pl}$ respectively are the tensor of the stress and the incremental plastic strain; V is the total volume of the SPD; and $\bar{t}$ is the loading duration.

4.2 Model verification

To verify the FE model of the SPD used in this study, this model was compared with the FE model presented in the study by Deng *et al*. (2014). The dimensions of the SPD model are shown in Fig. 3(a). The SPD is a 200 × 200 mm square plate and is made of a low yield steel which is known as LY255. The SPD thickness is also equal to 12 mm. In order to prevent the low cycle fatigue failure in the welded zone of the top and bottom SPD, the width of these zones was increased by 60 mm. The material properties of the SPD model are shown in Table 1.

In the nonlinear analysis of the SPD FE model, the best balance between accuracy and computational cost depends

Table 1 Parameters of numerical material law (MPa) (Deng *et al*. 2014)

C_1	γ_1	C_2	γ_2	C_3	γ_3	σ_0
20,000	400	18,000	500	1200	2	235

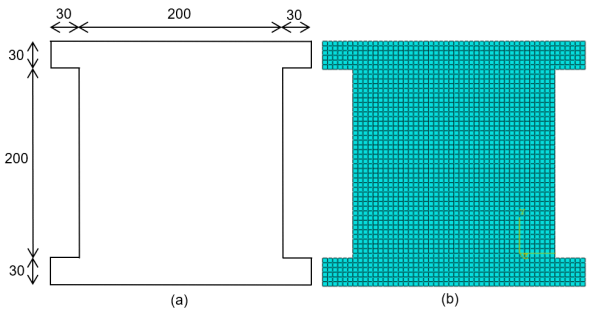

Fig. 3 (a) Dimensions of the SPD in mm; (b) meshing configuration of the FE model of the SPD

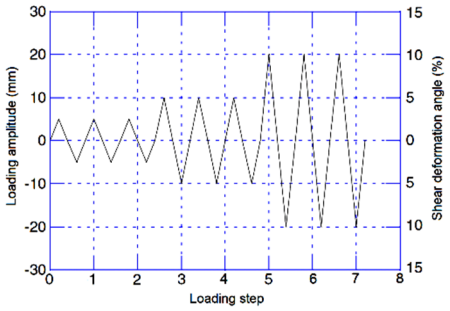

Fig. 4 Cyclic loading protocol for the FE analysis of the SPD (Deng *et al*. 2014)

on the size of meshes. As recommended by Deng *et al*. (2014), the size of mesh elements was assumed to be 5 mm. The dimensions and mesh configuration of the FE model for the SPD is shown in Fig. 3.

A cyclic loading pattern shown in Fig. 4 (Deng *et al*. 2014) was considered to be exerted on the SPD. The cyclic loading was applied at the upper edge of the top welded zone of the SPD.

After the elasto-plastic analysis of the SPD subjected to the cyclic loading, the distribution of *PEEQ* obtained in this study is compared with that of the model reported in the work (Deng *et al*. 2014) and the results are shown in Fig 5. As can be seen from Fig. 5, the *PEEQ* distribution and its maximum value ($PEEQ_{max}$) of the FE model of this study is in a good agreement with that of the model presented by Deng *et al*. (2014). Thus, the results demonstrate the accuracy of the FE model used in this study.

5. WLS-SVM approach

Support vector machine (SVM)-based models as a type of supervised learning techniques have been proposed by mapping input data to the higher-dimensional feature spaces. Unlike artificial neural networks, SVMs are more stable and require much computational effort and a few parameters for the construction of a prediction model. These techniques can also be trained by a limited number of samples when a large number of data is not available, or constructing a large number of data requires a time-consuming process. In recent years, the WLS-SVM method has been introduced as a high accurate and robust prediction model and its successful applications have been demonstrated in solving many structural engineering problems (Khatibinia *et al*. 2013, 2015, Gharehbaghi and Khatibinia 2015, Yazdani *et al*. 2016, Gharehbaghi *et al*. 2019). This model is briefly expressed in this section.

Suykens *et al*. (2002) proposed the WLS-SVM model for solving the highly non-linear and small-sample problems. This model is described as an optimization problem in a primal weight space as follows (Suykens *et al*. 2002)

$$\begin{aligned} &\text{Minimize} \quad J(\boldsymbol{\omega},\xi) = \frac{1}{2}\boldsymbol{\omega}^T\boldsymbol{\omega} + \frac{1}{2}\gamma\sum_{i=1}^{n} w_i\xi_i^2 \\ &\text{Subjest to} \quad y_i = \boldsymbol{\omega}^T\phi(\boldsymbol{x}_i) + b + \xi_i; \quad i = 1,2,\ldots,n \end{aligned} \tag{16}$$

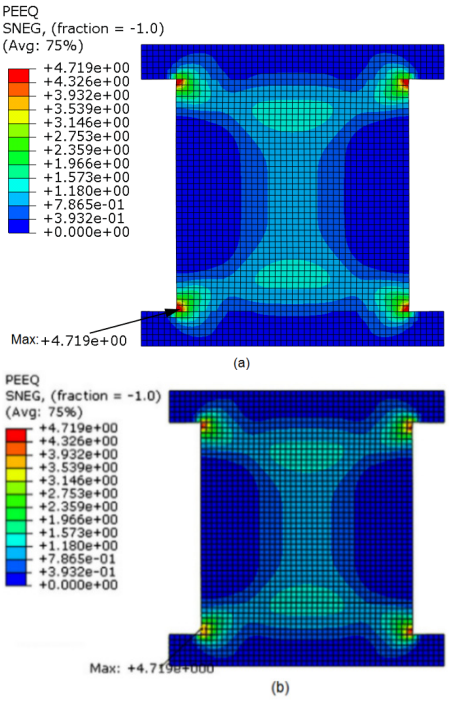

Fig. 5 Comparison of the distribution of *PEEQ* between (a) this study; and (b) the study implemented by Deng *et al*. (2014)

in which $\{\boldsymbol{x}_i, y_i\}_{i=1}^{n}$ is a training data set, $\boldsymbol{x}_i \in R^n$ is input data, and $y_i \in R$ is output data. $\phi(.):R^n \rightarrow R^d$ is a function which maps the input data into a high-dimensional space. $\boldsymbol{\omega} \in R^d$ is expressed as a weight vector in the primal weight space. $\xi_i \in R$ and $b \in R$ are the error variable and the bias term, respectively.

The solution of the dual problem defined in Eq. (16) is obtained by the Lagrange multiplier technique as

$$\begin{aligned} &L(\boldsymbol{\omega}, b, \xi, \boldsymbol{\alpha}) \\ &= J(\boldsymbol{\omega}, \xi) - \sum_{i=1}^{n} \alpha_i(\boldsymbol{\omega}^T\phi(\boldsymbol{x}_i) + b + \xi_i - y_i) \end{aligned} \tag{17}$$

The Karush-Kuhn-Tucker (KKT) conditions are used for solving the Eq. (17). Hence, by employing the KKT condition and eliminating $\boldsymbol{\omega}$ and ξ, the set of linear equations is obtained as follows

$$\begin{bmatrix} \Omega + \boldsymbol{V}_\gamma & \mathbf{1}_n^T \\ \mathbf{1}_n & \mathbf{0} \end{bmatrix} \begin{bmatrix} \boldsymbol{\alpha} \\ b \end{bmatrix} = \begin{bmatrix} \boldsymbol{y} \\ 0 \end{bmatrix} \tag{18}$$

where $\boldsymbol{V}_\gamma = diag\{1/\gamma\bar{v}_1, \ldots, 1/\gamma\bar{v}_n\}$; Ω is $n \times n$ Hessian vector which is expressed as $\Omega_{i,j} = \langle\phi(\boldsymbol{x}_i), \phi(\boldsymbol{x}_j)\rangle_H = K(\boldsymbol{x}_i, \boldsymbol{x}_j)$. $K(.,.)$ is considered a kernel function. α and b are the solutions to the set of linear equations.

In this study, the radial basis function as a most popular kernel function of the WLS-SVM model is selected and is defined as

$$K(\boldsymbol{x}_i, \boldsymbol{x}_j) = exp\left(-\frac{\|\boldsymbol{x}_i - \boldsymbol{x}_j\|^2}{2\sigma^2}\right) \tag{19}$$

Therefore, the output data is predicted by the WLS-SVM model as follows

$$y(\boldsymbol{x}) = \sum_{i=1}^{n} \alpha_i K(\boldsymbol{x}_i, \boldsymbol{x}) + b \tag{20}$$

6. Predictive model of SPD responses

Since the shape optimization problem of the SPD defined above (see section 3) requires a large number of the inelastic FE analyses in the ABAQUS software, expensive computational efforts are needed. In order to eliminate the drawback, a predictive model based on the WLS-SVM approach was employed in the optimization procedure to estimate the inelastic responses of the SPD with sufficient accuracy. As such, two training and testing sets including a number of different SPD samples in term of design variables were provided to train and test the WLS-SVM model. The SPD samples were randomly generated by Latin Hypercube Design (LHD) sampling (McKay *et al*. 1979) method. In these samples, the design variables and the objective function defined in Eq. (2) were selected as the input and output data set in the WLS-SVM model, respectively. The input and output sets of the WLS-SVM model are defined as follows

$$\boldsymbol{I}_{WLS-SVM} = \{\boldsymbol{x}_1, \boldsymbol{x}_2, \ldots, \boldsymbol{x}_{ns}\} \tag{21}$$

$$\boldsymbol{O}_{WLS-SVM} = \{y_1, y_2, \ldots, y_{ns}\} \tag{22}$$

where $\boldsymbol{I}$ and $\boldsymbol{O}$ are expressed as the input and output vectors of the WLS-SVM model, respectively. *ns* is the number of samples.

The flowchart shown in Fig. 6 depicts the procedure of the data generation by linking ABAQUS to MATLAB (2018). Each of input vectors ($\boldsymbol{x}_i$) defined based on the design variables in Eq. (2) was firstly considered for the construction of an SPD FE model in the framework of a Python script. This step is called the ABAQUS pre-processing module. In the next step, the FE analysis of the SPD subjected to cyclic loading was also conducted. Finally, the value of objective function was obtained in ABAQUS post-processing module.

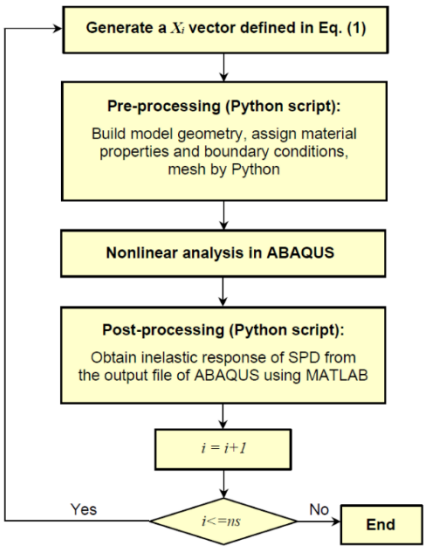

Fig. 6 Flowchart of dataset generation

In order to assess the accuracy of the predicted response of the SPD FE analysis by the WLS-SVM model, three statistical metrics including the mean absolute percentage error (*MAPE*), the relative root-mean-squared error (*RRMSE*) and the absolute fraction of variance (r^2) are employed in the testing process of the WLS-SVM model as

$$MAPE = \frac{1}{n_t} \sum_{i=1}^{n_t} 100 \times \left| \frac{a_i - p_i}{a_i} \right| \tag{23}$$

$$RRMSE = \sqrt{\frac{n_t \sum_{i=1}^{n_t} (a_i - p_i)^2}{(n_t - 1) \sum_{i=1}^{n_t} a_i^2}} \tag{24}$$

$$r^2 = 1 - \frac{\sum_{i=1}^{n_t} (a_i - p_i)^2}{\sum_{i=1}^{n_t} p_i^2} \tag{25}$$

where a and p are the actual and the predicted value, respectively; and n_t is the number of samples used for performance validation of the model. It is worth mentioning that the smaller *RRMSE* and *MAPE* and the larger r^2 are indicative of better performance generality.

7. Numerical example

In this section, the optimum shape design of an SPD subjected to the cyclic loading is considered as the worked example. The cyclic loading used in this study is shown in Fig. 4. The SPD is a rectangular plate with the height of 200 mm, width of 300 mm and a uniform thickness of t equal to 12 mm. In addition, it is assumed that this plate is made of low yield steel as LY255 with the yield and ultimate stress of 20 and 30 kPa, respectively. To implement the optimization process, the population size (n_{ps}) and the maximum number of iterations (l_{max}) of WOA were set to 30 and 200, respectively. The lower and upper bounds of the design variables defined in Eq. (1) are shown in Table 2. The optimization process is performed by a Core i5 Duo 3.0 GHz CPU and the time of all computations is evaluated in clock time.

7.1 Training and testing the WLS-SVM model

In order to develop a predictive model of WLS-SVM for each of the objective functions, first, a dataset including 200 samples of the design variables (i.e., the SPDs with

Table 2 Lower and upper bounds for the dimensions of the SPD

Parameter	Lower bound (mm)	Upper bound (mm)
h	40	130
L	20	50

Table 3 Performance metrics for the WLS-SVM model in the testing mode

Objective function	*MAPE*	*RRMSE*	r^2
F_1	2.9175	0.0361	0.9987
F_2	3.9472	0.0535	0.9971

different shapes) was provided using the LHD sampling technique. Then, each of these samples was subjected to the cyclic loading pattern shown in Fig. 4. The samples (randomly generated SPDs) were analyzed in the ABAQUS software and their responses including *ALLPD* and $PEEQ_{max}$ were obtained. Based on these responses, the actual values of the objective functions defined in Eqs. (3) and (4) were computed. The elapsed time of the data generation was about 2,000 min (i.e., about 34 hours). Finally, 140 (i.e., 70% of total) and 60 (i.e., 30% of total) samples were randomly selected to train a WLS-SVM model and to test its performance generality. In the training phase, the optimum values of γ and σ were found by using a k-fold cross-validation and the grid searching method (Suykens *et al*. 2002). The results of testing the WLS-SVM model are shown in Table 3.

As can be seen from Table 3, the low values of *MAPE* and *RRMSE* and the high value of r^2 demonstrate the high accuracy of the WLS-SVM model. Fig. 7 shows the scatter diagrams for the actual and predicted values of the two objective functions in the testing mode. It can be observed from Fig. 7 that the data predicted by the WLS-SVM model is closer to the corresponding data obtained from ABQUS. Since the predictive models accurately predict the inelastic responses of the SPDs for determining the objective functions, the WLS-SVM model can be used in the optimization procedure instead of ABAQUS software. Hence, the WLS-SVM model can effectively reduce the overall computational time and cost therefore. It is noted that the elapsed time of training and testing the WLS-SVM model for objective functions (i.e., F_1 and F_2) was 1.6 and 1.63 min, respectively.

Table 4 The dimensions of the optimum shaped-SPD obtained for the two objective functions

Dimensions (mm)	Objective function		$100\times(F_2\text{-}F_1)/F_1$ (%)
	F_1	F_2	
h	90.394	92.330	2.14
L	44.449	44.271	-0.40

Table 5 Comparison of the objective functions for the optimum shaped-SPD obtained by FE analysis and WLS-SVM

Objective function	FE analysis	WLS-SVM	Error (%)
F_1	1.685	1.716	1.85
F_2	112.116	102.487	8.60

7.2 The results of shape optimization

To find the optimum shape of the SPD, first, 10 independent runs were conducted for each of the objective functions. Then, the best solution corresponding to each objective function was adopted as the global (or near global) optimal solution. The optimum dimensions corresponding to each of the objective functions are listed in Table 4. It can be seen from Table 4 that the optimum shape of the SPD for both objective functions are different. The dimension h for F_1 is 2.14% greater than that of F_2; and L is 0.4% smaller than that of F_2.

In order to evaluate the feasibility and efficiency of the optimum-shaped SPDs obtained by the combination of WOA and WLS-SVM, the optimum designs presented in Table 4 were firstly analyzed subjected to the cyclic loading by using ABAQUS. Then, their actual response of the SPD (i.e., the objective function) was calculated. The actual and predicted responses were compared and shown in Table 5.

As can be seen from Table 5, the percentage of errors for the WOA algorithm is 1.85% and 8.60% respectively for the objective functions (i.e., F_1 and F_2). These low errors indicate that the WLS-SVM model could reliably be used in

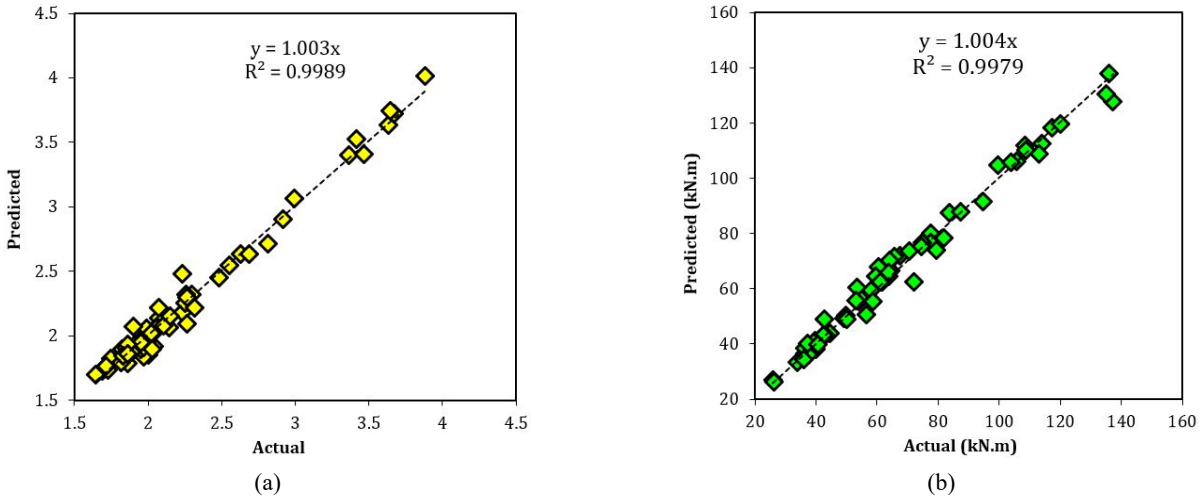

(a) (b)

Fig. 7 Exact versus predicted value of (a) F_1 objective function; and (b) F_2 objective function in the testing mode

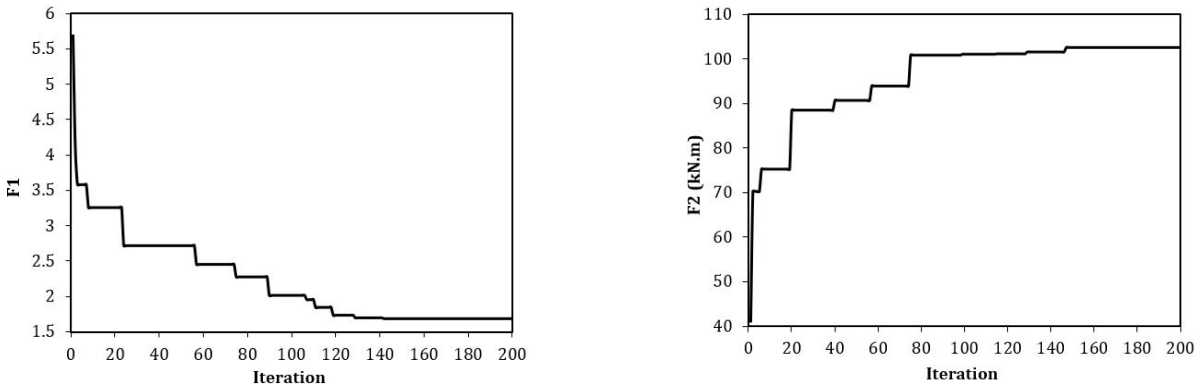

(a) (b)

Fig. 8 The convergence history for (a) F_1 objective function; (b) F_2 objective function

Table 6 Comparison of the inelastic responses of the optimum shaped-SPD corresponding to each the objective function

Inelastic response	Initial SPD	Objective function	
		F_1	F_2
$PEEQ_{max}$	6.044	1.685 (-72.12%)	1.669 (-72.24%)
ALLPD (kN.m)	198.171	185.311 (-6.49%)	188.083 (-5.1%)
ALLPD to $PEEQ_{max}$ (kN.m)	32.788	109.792 (+234.8%)	112.692 (+243%)

the optimization procedure instead of the FE analysis by means of ABAQUS as it could accurately predict the inelastic responses of the USSD. The convergence history of both F_1 and F_2 objective functions are depicted in Fig. 8.

7.3 Performance evaluation of the optimized SPDs

In order to assess the cyclic behavior of the optimum shapes of the SPD determined based on each of the objective functions, their performance subjected to the cyclic loading shown in Fig. 4 was compared with that of the initial one (i.e., the rectangular SPD mentioned before). For this purpose, first, the optimum-shaped SPDs corresponding to each of the objective functions were analyzed by ABAQUS. Then, their inelastic responses including *ALLPD* and $PEEQ_{max}$ were obtained as listed in Table 6. As can be seen from Table 6, the $PEEQ_{max}$ of the optimized SPDs is 1.685 for objective function F_1, and is 1.669 for objective function F_2, which are almost 72.12% and 72.24% lower than that of the initial SPD shape. In addition, the *ALLPD* of the optimum-shaped SPDs is 185.311 kN.m for the objective function F_1, and is 188.083 kN.m for the objective function F_2, which are almost 6.49% and 5.1% lower than that of the initial SPD shape. These reductions are negligible in comparing with the significant improvements obtained in $PEEQ_{max}$. This is also confirmed by the results of *ALLPD* to $PEEQ_{max}$ ratio listed in Table 6. As shown in the table, the ratio for F_1 and F_2 is respectively improved almost 234.8 and 242% in comparison with that

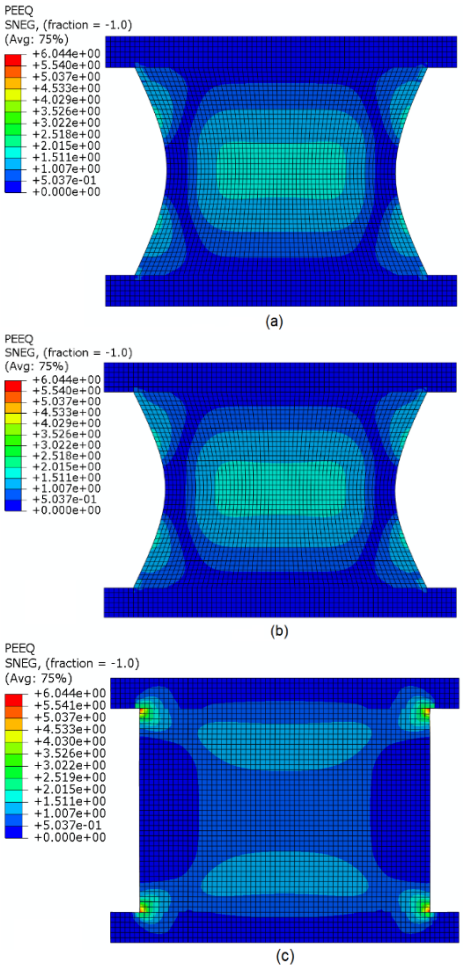

Fig. 9 The distribution of $PEEQ_{max}$ for the optimized SPD obtained based on (a) F_1 objective function; (b) F_2 objective function; and (c) the initial SPD

of the initial one. The distribution of $PEEQ_{max}$ over the optimum-shaped SPDs and initial shape under the cyclic loading is depicted in Fig. 9.

As shown in this figure, the distribution of $PEEQ_{max}$ for the optimum-shaped SPD is more uniform than that of the initial SPD. This issue is resulted in a smaller $PEEQ_{max}$ for the optimum shapes of the SPD compared with that of the

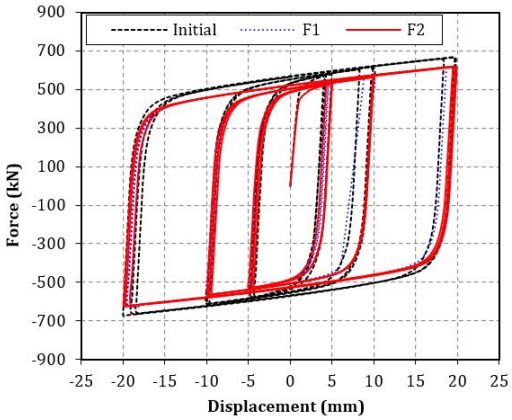

Fig. 10 Comparison of the hysteresis curve between the optimum shaped-SPD obtained based on F_1 and F_2 objective functions and the initial SPD

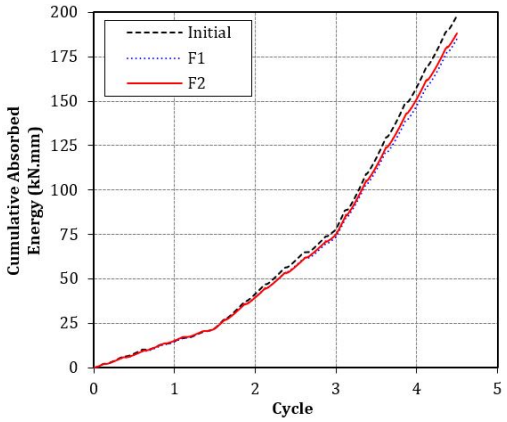

Fig. 11 Comparison of the hysteresis curve between the optimum shaped-SPD obtained based on F_1 and F_2 objective functions and the initial SPD

initial one. In the other word, the defined shape optimization problems render two optimum-shaped SPDs in which the damage concentration is avoided. The hysteresis curve for both optimum-shaped SPDs by using the objective functions of F_1 and F_2, and the initial SPD are also shown and compared in Fig. 10.

As can be seen from Fig. 10, the hysteretic curves of the optimum-shaped SPDs obtained based on both objective functions are almost the same, and they are slightly different than that of the initial SPD. In addition, the cumulative absorbing energy of the optimum-shaped SPDs and the initial SPD are shown in Fig. 11. Based on this figure, as resulted and discussed before, the cumulative absorbed energy through the loading cycles is slightly decreased for the optimum-shaped SPDs in comparing with the initial one.

Finally, all the results confirm that using the ratio of *ALLPD* to $PEEQ_{max}$ as the objective function F_2 results in an optimum-shape SPD which is more efficient in improving the low cycle fatigue performance under cyclic loading whilst a small reduction in its maximum *ALLPD* in comparing with the initial rectangular shaped SPD.

8. Conclusions

An accurate and low-computational effort framework was presented for the shape optimization of steel shear panel dampers (SPDs). To this end, an efficient computational approach consisting of a nature-inspired optimization algorithm and an accurate predictive tool was used. The whale optimization algorithm (WOA) was considered to implement the optimization process in order to find the optimum shape of SPDs. Since several inelastic cyclic analyses of SPDs were required during the optimization procedure, a weighted-support vector machine predictive approach, i.e., WLS-SVM, was adopted to develop a model for the prediction of the inelastic responses of the SPDs. In addition, to reach a more effective shape of SPD, two objective functions including the maximum equivalent plastic strain ($PEEQ_{max}$) and the ratio of energy dissipation through plastic deformation (*ALLPD*) to $PEEQ_{max}$ were chosen. To this end, the cubic version of Bezier curve was considered for the geometry of arc-shaped free edges on the left and right sides of the SPDs. The cyclic performance of the optimum-shaped SPDs obtained by the mentioned objective functions were compared with those of an initial rectangular shaped SPD. The following conclusions are obtained from this study:

- The WOA could find the optimum shaped SPDs well. In addition, the developed model by using the WLSSVM approach could accurately predict the required inelastic responses of the SPDs during the optimization procedure. Moreover, the elapsed time of the shape optimization procedure as a very time-consuming process was substantially reduced.
- The optimum shaped SPDs show more uniform *PEEQ*, lower $PEEQ_{max}$, and trivial reduction of maximum *ALLPD* in comparing with those of the initial rectangular shaped SPD. This issue reveals the capability of the shape optimization procedure implemented in this study.
- The results of the cyclic performance of the SPD optimum shapes confirm that maximizing the ratio of *ALLPD* to $PEEQ_{max}$ could be effectively used as the objective function of the shape optimization of SPDs rather than only minimizing $PEEQ_{max}$.

References

ABAQUS, (2003), Analysis user's manual-version 6.4, 19.2.2. Hbbit, Karlsson & Sorensen, Inc.

Akbari, H.A. and Mofid, M. (2015), "On the experimental and numerical study of braced steel shear panels", *Struct. Des. Tall. Spec.*, **24**(14), 853-872. https://doi.org/10.1002/tal.1215

Aoki, T., Liu, Y., Takaku, T., Uenoya, M. and Fukumoto, Y. (2007), "Experimental investigation of tapered shear-type seismic devices for bridge bearings", In: *Pacific Structural Steel Conference*, *Steel Structures in Natural Hazards*, Wairakei, New Zealand.

Bilondi, M.R.S., Yazdani, H. and Khatibinia, M. (2018), "Seismic energy dissipation-based optimum design of tuned mass dampers", *Struct. Multidiscipl. Optimi.*, **58**(6), 2517-2531. https://doi.org/10.1007/s00158-018-2033-0

Boggs, P.T. and Tolle, J.W. (1995), "Sequential quadratic programming", *Acta. Numeric.*, **4**, 1-52. https://doi.org/10.1017/S0962492900002518

Brando, G. and De Matteis, G. (2014), "Design of low strength-high hardening metal multi-stiffened shear plates", *Eng. Struct.*, **60**, 2-10. https://doi.org/10.1016/j.engstruct.2013.12.005

Chan, R.W., Albermani, F. and Kitipornchai, S. (2013), "Experimental study of perforated yielding shear panel device for passive energy dissipation", *J. Constr. Steel Res.*, **91**, 14-25. https://doi.org/10.1016/j.jcsr.2013.08.013

Choi, I.R. and Park, H.G. (2010), "Hysteresis model of thin infill plate for cyclic nonlinear analysis of steel plate shear walls", *J. Struct. Eng.*, **136**(11), 1423-1434. https://doi.org/10.1061/(ASCE)ST.1943-541X.0000244

De Matteis, G., Mazzolani, F. and Panico, S. (2008), "Experimental tests on pure aluminium shear panels with welded stiffeners", *Eng. Struct.*, **30**(6), 1734-1744. https://doi.org/10.1061/(ASCE)ST.1943-541X.0000244

De Matteis, G., Sarracco, G. and Brando, G. (2009), "Bracing type pure aluminium stiffened shear panels: an experimental study", *Adv. Steel. Constr.*, **5**(2), 106-119.

De Matteis, G., Brando, G. and Mazzolani, F.M. (2011), "Hysteretic behaviour of bracing-type pure aluminium shear panels by experimental tests", *Earthq. Eng. Struct. Dyn.*, **40**(10), 1143-1162. https://doi.org/10.1002/eqe.1079

De Matteis, G., Sarracco, G. and Brando, G. (2016), "Experimental tests and optimization rules for steel perforated shear panels", *J. Constr. Steel Res.*, **123**, 41-52. https://doi.org/10.1016/j.jcsr.2016.04.025

Deng, K., Pan, P., Sun, J., Liu, J. and Xue, Y. (2014), "Shape optimization design of steel shear panel dampers", *J. Constr. Steel Res.*, **99**, 187-193. https://doi.org/10.1016/j.jcsr.2014.03.001

Egorova, N., Eatherton, M.R. and Maurya, A. (2014), "Experimental study of ring-shaped steel plate shear walls", *J. Constr. Steel Res.*, **103**, 179-189. https://doi.org/10.1016/j.jcsr.2014.09.002

Ene, D., Kishiki, S., Yamada, S., Jiao, Y., Konishi, Y., Terashima, M. and Kawamura, N. (2016), "Experimental study on the bidirectional inelastic deformation capacity of U-shaped steel dampers for seismic isolated buildings", *Earthq. Eng. Struct. Dyn.*, **45**(2), 173-192. https://doi.org/10.1002/eqe.2621

Faux, I.D. and Pratt, M.J. (1979), *Computational Geometry for Design and Manufacture*, Ellis Horwood Ltd.

Gharehbaghi, S. (2018), "Damage controlled optimum seismic design of reinforced concrete framed structures", *Struct. Eng. Mech., Int. J.*, **65**(1), 53-68. https://doi.org/10.12989/sem.2018.65.1.053

Gharehbaghi, S. and Khatibinia, M. (2015), "Optimal seismic design of reinforced concrete structures under time-history earthquake loads using an intelligent hybrid algorithm", *Earthq. Eng. Eng. Vibr.*, **14**(1), 97-109. https://doi.org/10.1007/s11803-015-0009-2

Gharehbaghi, S., Yazdani, H. and Khatibinia, M. (2019), "Estimating inelastic seismic response of reinforced concrete frame structures using a wavelet support vector machine and an artificial neural network", *Neural. Comput. Appl.*, **32**, 2975-2988. https://doi.org/10.1007/s00521-019-04075-2

Hamed, A.A. and Mofid, M. (2015), "On the equivalent simple models of braced steel shear panels", *Proceedings of the Institution of Civil Engineers-Structures and Buildings*, **168**(8), 570-577. https://doi.org/10.1680/stbu.14.00070

Hossain, M.R., Ashraf, M. and Albermani, F. (2011), "Numerical modelling of yielding shear panel device for passive energy dissipation", *Thin-Wall. Struct.*, **49**(8), 1032-1044. https://doi.org/10.1016/j.tws.2011.03.003

Jain, S., Rai, D.C. and Sahoo, D.R. (2008), "Postyield cyclic buckling criteria for aluminum shear panels", *J. Appl. Mech.*, **75**(2), 021015. https://doi.org/10.1115/1.2793135

Jiao, Y., Kishiki, S., Yamada, S., Ene, D., Konishi, Y., Hoashi, Y. and Terashima, M. (2015), "Low cyclic fatigue and hysteretic behavior of U-shaped steel dampers for seismically isolated buildings under dynamic cyclic loadings", *Earthq. Eng. Struct. Dyn.*, **44**(10), 1523-1538. https://doi.org/10.1002/eqe.2533

Jirasek, M. and Bazant, Z.P. (2001), *Inelastic Analysis of Structures*, John Wiley & Sons.

Kang, T.H.K., Martin, R.D., Park, H.G., Wilkerson, R. and Youssef, N. (2013), "Tall building with steel plate shear walls subject to load reversal", *Struct. Des. Tall. Spec.*, **22**(6), 500-520. https://doi.org/10.1002/tal.700

Khatibinia, M., Fadaee, M.J., Salajegheh, J. and Salajegheh, E. (2013), "Seismic reliability assessment of RC structures including soil–structure interaction using wavelet weighted least squares support vector machine", *Reliab. Eng. Syst. Saf.*, **110**, 22-33. https://doi.org/10.1016/j.ress.2012.09.006

Khatibinia, M., Gharehbaghi, S. and Moustafa, A. (2015), "Seismic reliability-based design optimization of reinforced concrete structures including soil-structure interaction effects", In: *Earthquake Engineering-From Engineering Seismology to Optimal Seismic Design of Engineering Structures*, A. Moustafa, Editor., InTech: London, UK. pp. 267-304.

Khatibinia, M., Jalalipour, M. and Gharehbaghi, S. (2019), "Shape optimization of U-shaped steel dampers subjected to cyclic loading using an efficient hybrid approach", *Eng. Struct.*, **197**, 108874. https://doi.org/10.1016/j.engstruct.2019.02.005

Kishiki, S., Ohkawara, Y., Yamada, S. and Wada, A. (2008), "Experimental evaluation of cyclic deformation capacity of U-shaped steel dampers for base-isolated structures", *J. Struct. Constr. Eng.*, **73**(624), 333-340.

Lemaitre, J. and Chaboche, J.L. (1994), *Mechanics of Solid Materials*, Cambridge University Press.

Liu, Y. and Shimoda, M. (2013), "Shape optimization of shear panel damper for improving the deformation ability under cyclic loading", *Struct. Multidiscipl. Optimi.*, **48**(2), 427-435. https://doi.org/10.1007/s00158-013-0909-6

Liu, Y., Aoki, T., Takaku, T. and Fukumoto, Y. (2007), "Cyclic loading tests of shear panel damper made of low yield steel", *J. Struct. Constr. Eng. A*, **53**, 560-567.

Mahmoudi, M. and Abdi, M.G. (2012), "Evaluating response modification factors of TADAS frames", *J. Constr. Steel Res.*, **71**, 162-170. https://doi.org/10.1016/j.jcsr.2011.10.015

MATLAB (2018), *The Language of Technical Computing*, Vol. MathWorks, Inc. 2018: MathWorks, Incorporated.

McKay, M.D., Beckman, R.J. and Conover, W.J. (1979), "A comparison of three methods for selecting values of input variables in the analysis of output from a computer code", *Technometrics*, **21**(2), 239-245.

Mirjalili, S. and Lewis, A. (2016), "The whale optimization algorithm", *Adv. Eng. Softw.*, **95**, 51-67. https://doi.org/10.1016/j.advengsoft.2016.01.008

Nakashima, M., Iwai, S., Iwata, M., Takeuchi, T., Konomi, Sh., Akazawa, T. and Saburi, K. (1994), "Energy dissipation behaviour of shear panels made of low yield steel", *Earthq. Eng. Struct. Dyn.*, **23**(12), 1299-1313. https://doi.org/10.1002/eqe.4290231203

Ohsaki, M. and Nakajima, T. (2012), "Optimization of link member of eccentrically braced frames for maximum energy dissipation", *J. Constr. Steel Res.*, **75**, 38-44. https://doi.org/10.1016/j.jcsr.2012.03.008

Olhoff, N. (1995), *Structural and Multidisciplinary Optimization*: *Proceedings of the First World Congress of Structural and Multidisciplinary Optimization*, Goslar, Germany, May-June, Pergamon Press.

Rai, D.C., Annam, P.K. and Pradhan, T. (2013), "Seismic testing of steel braced frames with aluminum shear yielding dampers", *Eng. Struct.*, **46**, 737-747. https://doi.org/10.1016/j.engstruct.2012.08.027

Saeedi, F., Shabakhty, N. and Mousavi, S.R. (2016), "Seismic assessment of steel frames with triangular-plate added damping and stiffness devices", *J. Const. Steel Res.*, **125**, 15-25. https://doi.org/10.1016/j.jcsr.2016.06.011

Sahoo, D.R. and Rai, D.C. (2013), "Design and evaluation of seismic strengthening techniques for reinforced concrete frames with soft ground story", *Eng. Struct.*, **56**, 1933-1944. https://doi.org/10.1016/j.engstruct.2013.08.018

Sorace, S., Terenzi, G. and Mori, C. (2016), "Passive energy dissipation-based retrofit strategies for R/C frame water towers", *Eng. Struct.*, **106**, 385-398. https://doi.org/10.1016/j.engstruct.2015.10.038

Suykens, J.A., Brabanter, J.D., Lukas, L. and Vandewalle, J. (2002), "Weighted least squares support vector machines: robustness and sparse approximation", *Neurocomputing*, **48**(1-4), 85-105. https://doi.org/10.1016/S0925-2312(01)00644-0

Valizadeh, H., Sheidaii, M. and Showkati, H. (2012), "Experimental investigation on cyclic behavior of perforated steel plate shear walls", *J. Constr. Steel Res.*, **70**, 308-316. https://doi.org/10.1016/j.jcsr.2011.09.016

Vian, D., Bruneau, M. and Purba, R. (2009), "Special perforated steel plate shear walls with reduced beam section anchor beams. II: Analysis and design recommendations", *J. Struct. Eng.*, **135**(3), 221-228. https://doi.org/10.1061/(ASCE)0733-9445(2009)135:3(221)

Wong, K. (2008), "Seismic energy dissipation of inelastic structures with tuned mass dampers", *J. Eng. Mech.*, **134**(2), 163-172. https://doi.org/10.1061/(ASCE)0733-9399(2008)134:2(163)

Xu, F.H., Xu, Z.D. and Zhang, X.C. (2017), "Study on the space frame structures incorporated with magnetorheological dampers", *Smart. Struct. Syst., Int. J.*, **19**(3), 279-288. https://doi.org/10.12989/sss.2017.19.3.279

Yazdani, H., Khatibinia, M., Gharehbaghi, S. and Hatami, K. (2016), "Probabilistic performance-based optimum seismic design of RC structures considering soil–structure interaction effects", *ASCE-ASME J. Risk Uncertain. Eng. Syst. A Civ. Eng. Syst., Part A: Civil Eng.*, **3**(2), G4016004. https://doi.org/10.1061/AJRUA6.0000880

Zhang, C., Zhang, Z. and Shi, J. (2012a), "Development of high deformation capacity low yield strength steel shear panel damper", *J. Constr. Steel Res.*, **75**, 116-130. https://doi.org/10.1016/j.jcsr.2012.03.014

Zhang, C., Zhang, Z. and Zhang, Q. (2012b), "Static and dynamic cyclic performance of a low-yield-strength steel shear panel damper", *J. Constr. Steel Res.*, **79**, 195-203. https://doi.org/10.1016/j.jcsr.2012.07.030

Zhang, C., Zhu, J., Wu, M., Yu, J. and Zao, J. (2016), "The lightweight design of a seismic low-yield-strength steel shear panel damper", *Materials*, **9**(6), 424. https://doi.org/10.3390/ma9060424